Geosci. Model Dev., 8, 3055–3070, 2015
www.geosci-model-dev.net/8/3055/2015/
doi:10.5194/gmd-8-3055-2015
© Author(s) 2015. CC Attribution 3.0 License.

Geoscientific Model Development
Open Access

A soil diffusion–reaction model for surface COS flux: COSSM v1

W. Sun[1], K. Maseyk[2,a], C. Lett[2,b], and U. Seibt[1,2]

[1]Department of Atmospheric and Oceanic Sciences, University of California, Los Angeles, California, USA
[2]Institute of Ecology and Environmental Sciences, Université Pierre et Marie Curie, Paris, France
[a]now at: The Open University, Milton Keynes, UK
[b]now at: British Antarctic Survey, Cambridge, UK

Correspondence to: W. Sun (wu.sun@ucla.edu) and U. Seibt (useibt@ucla.edu)

Received: 18 May 2015 – Published in Geosci. Model Dev. Discuss.: 3 July 2015
Revised: 17 September 2015 – Accepted: 20 September 2015 – Published: 2 October 2015

Abstract. Soil exchange of carbonyl sulfide (COS) is the second largest COS flux in terrestrial ecosystems. A novel application of COS is the separation of gross primary productivity (GPP) from concomitant respiration. This method requires that soil COS exchange is relatively small and can be well quantified. Existing models for soil COS flux have incorporated empirical temperature and moisture functions derived from laboratory experiments but not explicitly resolved diffusion in the soil column. We developed a mechanistic diffusion–reaction model for soil COS exchange that accounts for COS uptake and production, relates source–sink terms to environmental variables, and has an option to enable surface litter layers. We evaluated the model with field data from a wheat field (Southern Great Plains (SGP), OK, USA) and an oak woodland (Stunt Ranch Reserve, CA, USA). The model was able to reproduce all observed features of soil COS exchange such as diurnal variations and sink–source transitions. We found that soil COS uptake is strongly diffusion controlled and limited by low COS concentrations in the soil if there is COS uptake in the litter layer. The model provides novel insights into the balance between soil COS uptake and production: a higher COS production capacity was required despite lower COS emissions during the growing season compared to the post-senescence period at SGP, and unchanged COS uptake capacity despite the dominant role of COS emissions after senescence. Once there is a database of soil COS parameters for key biomes, we expect the model will also be useful to simulate soil COS exchange at regional to global scales.

1 Introduction

Carbonyl sulfide (COS) is an atmospheric trace gas, with average concentration of around 480 pmol mol^{-1} (Montzka et al., 2007). COS uptake in leaves is coupled with CO_2 uptake through stomatal diffusion and hydrolysis mediated by carbonic anhydrase (CA) (Sandoval-Soto et al., 2005; Stimler et al., 2010; Seibt et al., 2010). Therefore plant COS flux measurements can be used to partition net carbon exchange into gross primary productivity (GPP) and respiration using the quantitative relationship between leaf COS and CO_2 uptake (Campbell et al., 2008; Asaf et al., 2013). Since the COS flux observed at ecosystem level and above is the sum of plant and soil fluxes, soil COS fluxes must be well quantified for COS-based flux partitioning. For many biomes where soils have active COS reactions, neglecting soil COS flux would result in significant biases of estimated GPP (Whelan et al., 2015). To enable COS-based flux partitioning, particularly at larger scales, a soil diffusion–reaction model is needed to generate estimates of soil COS exchange from soil parameters and environmental variables.

Laboratory studies have shown that soil COS uptake is a function of soil temperature and moisture, microbial CA enzyme activity, and ambient COS concentration (Kesselmeier et al., 1999; Van Diest and Kesselmeier, 2008). These empirical relationships were used by Kettle et al. (2002) to model global soil COS flux from climatological soil data. Recently, Berry et al. (2013) simulated global soil COS flux in the Simple Biosphere Model (SiB3) with the assumption that soil COS flux is a function of heterotrophic respiration and soil water-filled pore space fraction (WFPS). Here the effect of WFPS on diffusion was represented with an empiri-

cal function. Diffusion is not explicitly resolved in any existing model. The effect of a litter layer is also not considered. A litter layer may either act as a barrier for COS diffusion to the soil or participate in COS exchange. Plant litter has been found to contribute to the surface COS flux in forests (Kesselmeier and Hubert, 2002), with magnitudes comparable to that of soil uptake (Berkelhammer et al., 2014).

Existing models have also not considered the possibility of COS production in oxic, upland soils, based on the assumption that they usually behave as a COS sink (e.g., Kesselmeier et al., 1999; Yi et al., 2007; Van Diest and Kesselmeier, 2008; Liu et al., 2010a). However, soil COS fluxes varied between uptake and strong emissions in a wheat field depending on soil environmental variables (Maseyk et al., 2014). The presence of a compensation point for COS uptake also indicates that uptake and production can coexist in soils (Kesselmeier et al., 1999; Conrad and Meuser, 2000; Liu et al., 2010a).

Here we develop a diffusion–reaction model for soil COS flux, with four major advantages compared to previous empirical approaches:

1. Diffusion is explicitly resolved, providing a more realistic concentration-dependent uptake in the soil column.
2. The model accounts for flux activity in surface litter layers.
3. The model includes COS production terms.
4. Litter and soil COS uptake and production terms can be constrained or optimized using field data.

We evaluate the model using field data from a wheat field in the Southern Great Plains (Billings, OK, USA) and an oak woodland in the Santa Monica Mountains in southern California (Stunt Ranch Reserve, CA, USA).

2 Model description

2.1 The diffusion equation with source–sink terms

We construct a two-phase 1-D diffusion model with microbial COS source–sink terms in soil and litter layers to calculate surface COS fluxes. Diffusion of COS in the soil and litter is described by Fick's law in porous media,

$$\frac{\partial}{\partial t}\left[\left(k_{\mathrm{H}}\theta_{\mathrm{w}}+\theta_{\mathrm{a}}\right)C\right]=\frac{\partial}{\partial z}\left(D\frac{\partial C}{\partial z}\right)+S, \tag{1}$$

where θ_{w} and θ_{a} ($\mathrm{m^3\,m^{-3}}$ soil) are water-filled and air-filled porosities, C ($\mathrm{mol\,m^{-3}}$) is the gas concentration of COS, k_{H} (dimensionless) is Henry's law constant, D ($\mathrm{m^2\,s^{-1}}$) is the effective COS diffusivity in soil. The source–sink terms, S ($\mathrm{mol\,m^{-3}\,s^{-1}}$), are COS uptake and production in litter and soil. The boundary conditions are (1) concentration at the top boundary equals atmospheric concentration and (2) no flux at the bottom boundary.

For computational efficiency, diffusion in the aqueous phase is not prognostically evaluated but forced by the solubility equilibrium. By invoking Henry's law, the above equation assumes that the aqueous concentration is always in equilibrium with the gaseous concentration, ensuring mass balance. Approximating aqueous diffusive flux with this assumption does not significantly bias the surface flux (see Supplement), since aqueous diffusivity of COS is several orders of magnitude smaller than the gas-phase diffusivity (Ulshöfer et al., 1996).

Advective transport is not considered since the evaluation data sets were not affected by advection. However, advection effects on surface COS flux may not be negligible when there is strong wind pumping causing pressure fluctuations (Massman et al., 1997). Advective transport and prognostic aqueous processes (diffusion, dissolution and possibly ebullition) will be considered in future development once relevant data are collected.

2.2 Numerical implementation

2.2.1 Vertical grid

We use a face-centered finite-volume grid for discretizing the soil column, with 26 computational nodes down to 1 m depth. The vertical grid is constructed using an equation similar to that in the Community Land Model 4.5 (Oleson et al., 2013), which is more densely spaced at the upper boundary. This has advantages of resolving litter layers at the surface, and reducing the computational demand. The depths of the computational nodes are defined as

$$z_i=\exp\left(0.2i-5\right),\quad i=0,\ldots,N, \tag{2}$$

where $N=25$. The thicknesses of control volumes are

$$\Delta z_i=\begin{cases}\frac{z_0+z_1}{2}, & i=0\\ \frac{z_{i+1}-z_{i-1}}{2}, & i=1,\ldots,N-1\\ z_N-z_{N-1}, & i=N.\end{cases} \tag{3}$$

The depths of the layer interfaces are defined as

$$z_{i+1/2}=\begin{cases}\frac{z_i+z_{i+1}}{2}, & i=0,\ldots,N-1\\ z_N+\frac{z_N-z_{N-1}}{2}, & i=N.\end{cases} \tag{4}$$

The use of face-centered rather than node-centered control volumes generally gives better evaluation of diffusive fluxes across interfaces.

2.2.2 Discretization

We use the Crank–Nicolson method to discretize the diffusion–reaction equation, which ensures numerical stability when using large time steps (Crank and Nicolson, 1947). The method is implemented with second-order accuracy in space and in time. The discretized finite difference equations are a sparse linear system that can be easily solved.

We first discretize spatially Eq. (1) on the defined grid by integrating in each control volume (Durran, 2010; Tang and Riley, 2014),

$$\eta_i \Delta z_i \frac{\mathrm{d}C_i}{\mathrm{d}t} = \begin{cases} J_{\mathrm{a}\to 0} - J_{0\to 1} + S_0 \Delta z_0, & i = 0 \\ J_{i-1\to i} - J_{i\to i+1} + S_i \Delta z_i, & 1 \le i \le N-1 \\ J_{N-1\to N} + S_N \Delta z_N, & i = N, \end{cases} \tag{5}$$

where $\eta_i = (k_{\mathrm{H}}\theta_{\mathrm{w}} + \theta_{\mathrm{a}})$ at $z = z_i$ is a simplifying notation, $J_{\mathrm{a}\to 0}$ represents diffusive flux from the atmosphere to soil layer 0, and $J_{i-1\to i}$ represents diffusive flux from layer $i-1$ to layer i. The flux term J can be evaluated with a central difference scheme,

$$\begin{aligned} J_{i-1\to i} = & J_{i-1/2} = \left(-D\frac{\partial C}{\partial z}\right)_{i-1/2} \\ & = -D_{i-1/2}\frac{C_i - C_{i-1}}{z_i - z_{i-1}}. \end{aligned} \tag{6}$$

The diffusivity at the interface, $D_{i-1/2}$, can be interpolated linearly, $D_{i-1/2} = (D_i + D_{i-1})/2$, since the interface locates at the center of two computational nodes. For the ease of denotation, we define $G_{i-1/2} = D_{i-1/2}/(z_i - z_{i-1})$ as the conductance at the interface.

The flux at the topmost layer is thus

$$J_{\mathrm{a}\to 0} = -D_{\mathrm{a}\to 0}\frac{C_0 - C_{\mathrm{a}}}{z_0 - 0} = -G_{\mathrm{a}\to 0}(C_0 - C_{\mathrm{a}}). \tag{7}$$

Again, $D_{\mathrm{a}\to 0}$ is the diffusivity at the soil–atmosphere boundary, and $G_{\mathrm{a}\to 0}$ is the conductance. We use the harmonic mean of soil diffusivity D_0 and air diffusivity D_{a} for $D_{\mathrm{a}\to 0}$, following the conductance model in Tang and Riley (2013),

$$D_{\mathrm{a}\to 0} = \frac{2}{\frac{1}{D_0} + \frac{1}{D_{\mathrm{a}}}}. \tag{8}$$

By rewriting Eq. (5) in a matrix form, we obtain an ordinary differential equation (ODE) system for time,

$$\mathbf{A}\frac{\mathrm{d}}{\mathrm{d}t}\mathbf{C} = \mathbf{B}\mathbf{C} + \mathbf{S}, \tag{9}$$

where

$$\mathbf{C} = (C_0, C_1, \ldots, C_N)^{\mathbf{T}},$$

$$\mathbf{A} = \mathrm{diag}\,(\eta_0 \Delta z_0, \eta_1 \Delta z_1, \ldots, \eta_N \Delta z_N),$$

$$\mathbf{B} = \begin{pmatrix} -G_{\mathrm{a}\to 0} - G_{1/2} & G_{1/2} & 0 & \cdots & 0 & 0 & 0 \\ G_{1/2} & -G_{1/2} - G_{3/2} & G_{3/2} & \cdots & 0 & 0 & 0 \\ \vdots & \vdots & \vdots & \ddots & \vdots & \vdots & \vdots \\ 0 & 0 & 0 & \cdots & G_{N-3/2} & -G_{N-3/2} - G_{N-1/2} & G_{N-1/2} \\ 0 & 0 & 0 & \cdots & 0 & G_{N-1/2} & -G_{N-1/2} \end{pmatrix},$$

$$\mathbf{S} = \left(S_0 \Delta z_0 + \frac{D_{\mathrm{a}\to 0}}{z_0} C_{\mathrm{a}}, S_1 \Delta z_1, \ldots, S_N \Delta z_N\right)^{\mathbf{T}}. \tag{10}$$

The above linear ODE system is then discretized at time step $t = (n + 1/2)\Delta t$:

$$\mathbf{A}\frac{\mathbf{C}_{n+1} - \mathbf{C}_n}{\Delta t} = \mathbf{B}\frac{\mathbf{C}_{n+1} + \mathbf{C}_n}{2} + \mathbf{S}. \tag{11}$$

Therefore, the evolution in time is,

$$\mathbf{C}_{n+1} = (2\mathbf{A} - \Delta t\mathbf{B})^{-1}\left[(2\mathbf{A} + \Delta t\mathbf{B})\mathbf{C}_n + 2\Delta t\mathbf{S}\right]. \tag{12}$$

At each time step, the concentration profile is evolved to the next time step with the diffusion–reaction operator. Thus, the model can simulate transient conditions in real time.

2.3 Parameterization

2.3.1 Diffusivities

The diffusivity of COS in soil media (D, $\mathrm{m^2\ s^{-1}}$) is calculated following Moldrup et al. (2003),

$$\frac{D}{D_{\mathrm{m}}} = \theta_{\mathrm{a}}^2 \left(\frac{\theta_{\mathrm{a}}}{\theta_{\mathrm{sat}}}\right)^{3/b} \left(\frac{T}{T_{\mathrm{ref}}}\right)^n, \tag{13}$$

where θ_{sat} ($\mathrm{m^3\ m^{-3}}$) is the soil total porosity ($\theta_{\mathrm{sat}} = \theta_{\mathrm{a}} + \theta_{\mathrm{w}}$), D_{m} ($\mathrm{m^2\ s^{-1}}$) is the COS-air diffusivity at $T_{\mathrm{ref}} = 25\,^\circ\mathrm{C}$ and 1 atm, $n = 1.5$ (Bird et al., 2002), and b is parameterized with a water retention function (Wingate et al., 2008; Clapp and Hornberger, 1978). We assume that the same function holds for litter layer diffusivity since litter is also a porous medium like the soil.

For COS, D_{m} is calculated as $1.337 \times 10^{-5}\ \mathrm{m^2\ s^{-1}}$ at 25 °C and 1 atm, based on the theoretical CO_2 / COS diffusivity ratio of 1.21 derived in Seibt et al. (2010) from the Chapman–Enskog kinetic theory, and the molecular diffusivity of CO_2 ($1.618 \times 10^{-5}\ \mathrm{m^2\ s^{-1}}$, 25 °C and 1 atm) is calculated from Massman (1998).

2.3.2 COS solubility function

In solubility equilibrium, the chemical potentials of COS in gas phase (μ_{g}) and in aqueous solution (μ_{aq}) are equal:

$$\begin{aligned} \mu_{\mathrm{g}} = & \mu_{\mathrm{g}}^{\ominus}(T) + RT\ln\frac{p}{p^{\ominus}} + RT\ln\phi = \\ & \mu_{\mathrm{aq}}^{*}(T, p) + RT\ln x + RT\ln\gamma = \mu_{\mathrm{aq}}, \end{aligned} \tag{14}$$

where p is the partial pressure in gas phase, x is the molar fraction in aqueous phase, ϕ is the fugacity coefficient, γ is the activity coefficient, and $p^{\ominus}$ is the standard pressure. Here, $\mu_{\mathrm{g}}^{\ominus}$ and μ_{aq}^{*} are both chemical potentials under chosen standard conditions. Note that $\mu_{\mathrm{g}}^{\ominus}$ depends only on temperature, whereas μ_{aq}^{*} depends on both temperature and pressure.

For a dilute solution, as $x \to 0$ and $p/p^{\ominus} \to 0$, we have $\phi \to 1$ and $\gamma \to 1$. This is valid for COS in natural environments because its molar fraction is only $\sim 10^{-10}$ in the atmosphere (Montzka et al., 2007) and $\sim 10^{-12}$ in seawater (Ulshöfer et al., 1996; Von Hobe et al., 1999). Therefore,

$$\mu_{\mathrm{aq}}^{*} - \mu_{\mathrm{g}}^{\ominus} = -RT\ln\frac{x}{p/p^{\ominus}} \equiv -RT\ln k_{\mathrm{H},xp}, \tag{15}$$

where $k_{\mathrm{H},xp}$ is Henry's law constant defined as the ratio of aqueous-phase molar fraction to gas-phase partial pressure.

According to the van't Hoff equation,

$$\frac{\partial \ln k_{\mathrm{H},xp}}{\partial T} = \frac{\Delta_{\mathrm{sol}} H_{\mathrm{m}}^{\ominus}}{RT^2}, \tag{16}$$

where $\Delta_{\mathrm{sol}} H_{\mathrm{m}}^{\ominus}$ is the standard partial molar enthalpy of dissolution. We assume that it is constant within the temperature range of ambient conditions. With respect to a reference state T_0, integrating yields

$$\ln k_{\mathrm{H},xp} = -\frac{\Delta_{\mathrm{sol}} H_{\mathrm{m}}^{\ominus}}{R}\left(\frac{1}{T} - \frac{1}{T_0}\right). \tag{17}$$

Temperature dependence of $k_{\mathrm{H},xp}$ can thus be described by the following function, with A and B constants:

$$k_{\mathrm{H},xp} = \exp\left(\frac{A}{R} + \frac{B}{RT}\right). \tag{18}$$

The dimensionless Henry law constant, $k_{\mathrm{H},cc}$, is defined as the ratio of aqueous molar concentration to gaseous molar concentration.

$$k_{\mathrm{H},cc} \equiv \frac{c_{\mathrm{aq}}}{c_{\mathrm{g}}} = \frac{\rho_{\mathrm{w}} x / M_{\mathrm{w}}}{p/(RT)} = \frac{\rho_{\mathrm{w}} RT}{M_{\mathrm{w}} p^{\ominus}} \cdot \frac{x}{p/p^{\ominus}} = \frac{\rho_{\mathrm{w}} RT}{M_{\mathrm{w}} p^{\ominus}} k_{\mathrm{H},xp} = T \exp\left(\frac{A}{R} + \ln\frac{\rho_{\mathrm{w}} RT}{M_{\mathrm{w}} p^{\ominus}} + \frac{B}{RT}\right). \tag{19}$$

Thus, we can build a nonlinear regression model for temperature dependence of the dimensionless Henry law constant:

$$k_{\mathrm{H},cc}(T) = (T/\mathrm{K}) \exp\left(\alpha + \frac{\beta}{T/\mathrm{K}}\right). \tag{20}$$

Using Elliott et al. (1989) data for the regression (Fig. 2), we obtained that $\alpha = -20.00^{+1.48}_{-1.46}$, and $\beta = 4050^{+424}_{-430}$ (95 % confidence interval).

2.3.3 Soil fluxes

Because both COS uptake and production activities exist in soils and the net COS flux exhibits a linear response to COS concentration (Kesselmeier et al., 1999; Conrad and Meuser, 2000), we assume that uptake and production are separable terms.

Soil COS uptake (U) is formulated based on Michaelis–Menten kinetics, with dependence on soil temperature and moisture:

$$U = -V_{\mathrm{SU,max}} \cdot \frac{k_{\mathrm{H}} C}{K_{\mathrm{m}} + k_{\mathrm{H}} C} \cdot f(T) \cdot g(w), \tag{21}$$

where $K_{\mathrm{m}} = 1.9\,\mathrm{mol\,m^{-3}}$ is the Michaelis constant for COS hydrolysis by CA (Ogawa et al., 2013), $V_{\mathrm{SU,max}}$ ($\mathrm{mol\,m^{-3}\,s^{-1}}$) is the soil COS uptake capacity, and $f(T)$ and $g(w)$ are temperature and moisture limitation functions.

We assume that the temperature limitation function for soil COS uptake reflects the temperature dependence of enzyme activity, which is described as (Peterson et al., 2004; Daniel et al., 2010)

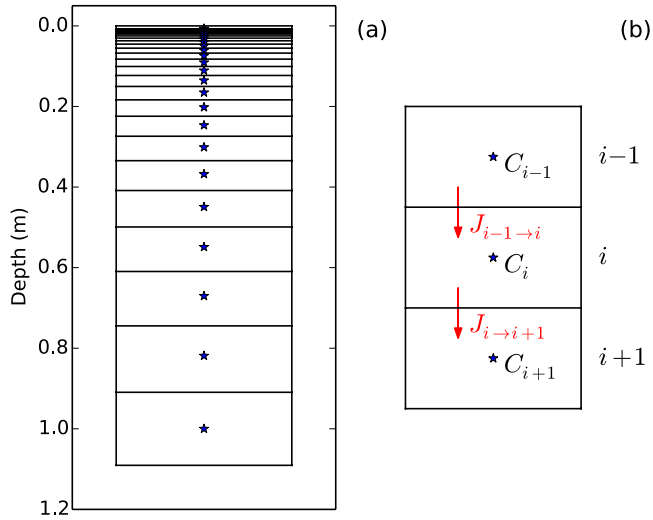

Figure 1. (a) The vertical finite-volume boxes and computational nodes (asterisk). **(b)** A schematic figure showing the diffusive fluxes (J) across boxes, which relate to concentration changes through mass balance.

$$f(T) = A_T \frac{T \exp\left(-\frac{\Delta^{\ddagger} G_{\mathrm{cat}}}{RT}\right)}{1 + \exp\left[-\frac{\Delta H_{\mathrm{eq}}}{R}\left(\frac{1}{T} - \frac{1}{T_{\mathrm{eq}}}\right)\right]}, \tag{22}$$

where $\Delta^{\ddagger} G_{\mathrm{cat}}$ ($\mathrm{J\,mol^{-1}}$) is the activation free energy of the transition state of the CA enzyme in terms of COS reactions, ΔH_{eq} ($\mathrm{J\,mol^{-1}}$) is the enthalpy change during conversion from activated to inactivated form of the enzyme, T_{eq} (K) is the temperature at which the concentrations of the activated enzyme and the inactivated enzyme are equal, A_T is the pre-exponential factor to normalize the equation so that $\max f(T) = 1$. The function has a temperature optimum, T_{opt}, defined at which the function reaches its maximum value. This temperature optimum is close to the parameter T_{eq} and always smaller than it (Peterson et al., 2004).

Other enzymes in soil microbes may also contribute to COS uptake, for example, COSase, nitrogenase and CS_2 hydrolase (Ogawa et al., 2013). These enzymes are not considered here due to lack of information on their kinetics and distribution in the microbial community. They are also unlikely to be as ubiquitous as CA.

Typical fit values of $\Delta^{\ddagger} G_{\mathrm{cat}}$ for a range of enzymes are between 51 and 88 $\mathrm{kJ\,mol^{-1}}$, whereas ΔH_{eq} varies from 86 to 826 $\mathrm{kJ\,mol^{-1}}$ (Daniel et al., 2010). We assume that $\Delta^{\ddagger} G_{\mathrm{cat}} = 84.10\,\mathrm{kJ\,mol^{-1}}$ (20.1 $\mathrm{kcal\,mol^{-1}}$) for CA-catalyzed COS hydrolysis, based on calculations of CA–COS nucleophilic attack, the rate-determining step of COS hydrolysis, which used $[(H_3N)_3Zn(OH)]^+$ as a structural analog of the active site of CA (Schenk et al., 2004).

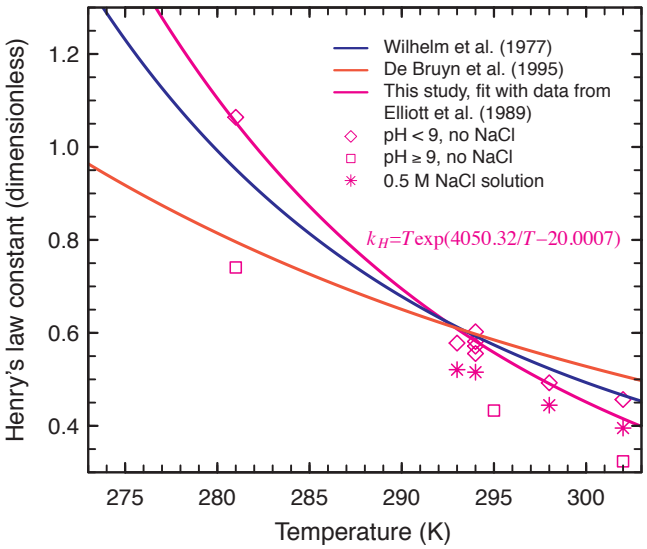

Figure 2. COS solubility function used in this study (pink), obtained from regression with Elliott et al. (1989) data (pink). Solubility data measured under pH < 9, non-saline conditions (pink diamonds) were used for the regression. Also plotted are the COS solubility functions from Wilhelm et al. (1977) and De Bruyn et al. (1995).

The temperature dependence (Eq. 22) has a similar mathematical form as that in Kesselmeier et al. (1999), but the temperature limitation of COS uptake is now linked to enzyme kinetics that can be determined in the laboratory. Using $\Delta^{\ddagger}G_{\mathrm{cat}} = 84.10\,\mathrm{kJ\,mol^{-1}}$, $\Delta H_{\mathrm{eq}} = 358.9\,\mathrm{kJ\,mol^{-1}}$, and $T_{\mathrm{eq}} = 293.14$ K, we can approximate the temperature function $\varphi(T)$ in Kesselmeier et al. (1999) (Fig. 3a). In this study, T_{eq} will be an adjustable parameter to fit temperature dependence for different soils (see Sect. 2.4.2 and Table 2).

For the parameterization of moisture dependence, we use a simple bell-shaped function, described by the form of the Rayleigh distribution function:

$$g(w) = A_w \cdot \frac{w}{w_{\mathrm{opt}}^2} \cdot \exp\left(-\frac{w^2}{w_{\mathrm{opt}}^2}\right), \tag{23}$$

where w_{opt} ($\mathrm{m^3\,m^{-3}}$) is the optimal water content for COS uptake, and A_W is the normalization factor such that $\max g(w) = 1$. The parameter w_{opt} can be adjusted to fit observed data (see Sect. 2.4.2 and Table 2). The function has a wider range than that in Kesselmeier et al. (1999) (Fig. 3b), and does not approach zero at high soil moisture. It represents the dependence of microbial uptake per se instead of a combination of diffusion and microbial uptake, because diffusion has already been accounted for. We found no empirical reason to assume that microbial uptake of COS be zero at high soil water content if it is not diffusion-limited.

Soil COS production is represented as an exponential function of temperature,

$$P = V_{\mathrm{SP,max}} \cdot \exp\left[k_T (T - T_{\mathrm{ref}})\right], \tag{24}$$

where $V_{\mathrm{SP,max}}$ ($\mathrm{mol\,m^{-3}\,s^{-1}}$) is the soil COS production capacity, k_T ($\mathrm{K^{-1}}$) is the temperature dependence factor that is equivalent to $Q_{10} = 1.9$, and $T_{\mathrm{ref}} = 25°\mathrm{C}$. The Q_{10} value here is set as the average value of the Q_{10} associated with the two regression lines of COS flux vs. temperature in Maseyk et al. (2014). Lab incubation of various soils has found that soil COS emissions generally exhibit exponential responses with temperature (Whelan et al., 2015). Although COS may be produced by both soil microbes and roots (Maseyk et al., 2014), we use a single production term in Eq. (24) due to a lack of data on the individual temperature responses of the different components.

2.3.4 Litter fluxes and litter properties

Litter was present at one of the model evaluation sites (Stunt Ranch). We obtained an equation for litter COS fluxes based on an incubation experiment with litter at the Stunt Ranch site (Sun et al., 2015),

$$F_{\mathrm{SL}} = -V_{\mathrm{LU,max}} \cdot \frac{k_{\mathrm{H}} C}{K_{\mathrm{m}} + k_{\mathrm{H}} C} \cdot \sinh\left(k_{\mathrm{L}} w_{\mathrm{L}}\right) + V_{\mathrm{LP,max}} \cdot \exp\left[k_T (T - T_{\mathrm{ref}})\right], \tag{25}$$

where $V_{\mathrm{LU,max}}$ ($\mathrm{mol\,m^{-3}\,s^{-1}}$) and $V_{\mathrm{LP,max}}$ ($\mathrm{mol\,m^{-3}\,s^{-1}}$) are the litter COS uptake and production capacities, k_T ($\mathrm{K^{-1}}$) is the temperature dependence factor for COS production equivalent to $Q_{10} = 1.9$, and k_{L} (dimensionless) is the moisture limitation factor for COS uptake. The hyperbolic sine function is chosen to describe the exponential dependence on litter water content.

Litter porosity is usually much larger than that of soils. In the model, the porosity at the grid point near the litter–soil interface is interpolated so as to prevent numerical instability caused by discontinuity (Fig. 4).

Temperatures of the litter layers were interpolated between soil and chamber air temperature by assuming a logarithmic temperature profile in the surface layer, according to mixing length theory (Prandtl, 1925). The roughness length was assumed to be 0.01 m (Stull, 1988).

2.4 Field data sets for model evaluation

2.4.1 Field sites

Southern Great Plains, OK (SGP): soil COS fluxes were measured from 1 April to 31 May 2012 in a wheat field at the ARM (Atmospheric Radiation Measurement) Southern Great Plains Central Facility (36.61° N, 97.49° W) near Billings, OK. The soils are mainly silt loam to clay loam, with 33 % sand, 22 % silt, and 45 % clay (Fischer et al.,

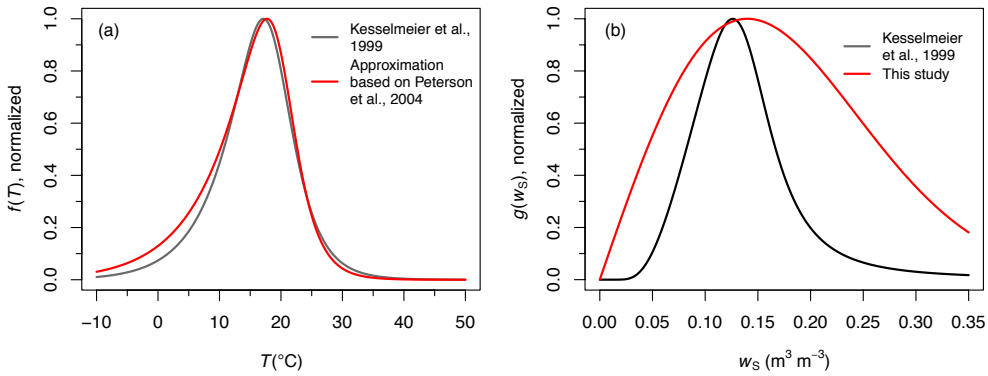

Figure 3. (a) Temperature dependence function of soil COS uptake (Eq. 22) with $\Delta H_{eq} = 358.9\,\mathrm{kJ\,mol^{-1}}$ and $T_{eq} = 20\,°\mathrm{C}$. **(b)** Moisture dependence function of soil COS uptake (Eq. 23) with $w_{opt} = 0.14\,\mathrm{m^3\,m^{-3}}$. Also plotted are the temperature and moisture dependence functions of Kesselmeier et al. (1999).

Table 1. COS solubility functions in the literature and in this study.

Reference	Model	Unit	Parameters
Wilhelm et al. (1977)	$\ln k_{H,xp} = \frac{A}{R} + \frac{B}{RT} + \frac{C}{R}\ln\frac{T}{K}$	$\mathrm{atm^{-1}}$	$A = -1839\ \mathrm{J\,K^{-1}\,mol^{-1}}$ $B = 99\,981\ \mathrm{J\,mol^{-1}}$ $C = 252\ \mathrm{J\,K^{-1}\,mol^{-1}}$
De Bruyn et al. (1995)	$\ln k_{H,xp} = \frac{A}{R} + \frac{B}{RT}$	$\mathrm{atm^{-1}}$	$A = 17552\ \mathrm{J\,K^{-1}\,mol^{-1}}$ $B = -124\ \mathrm{J\,mol^{-1}}$
This study with data from Elliott et al. (1989)	$k_{H,cc} = (T/K)\exp\left(\alpha + \frac{\beta}{T/K}\right)$	$\mathrm{mol\,mol^{-1}}$	$\alpha = -20.00$ $\beta = 4050$

2007). Further details on the site and data are provided in Maseyk et al. (2014).

Stunt Ranch, CA (SR): surface COS fluxes were measured from 1 April to 15 April 2013 in a Mediterranean oak woodland at the University of California Stunt Ranch Santa Monica Mountains Reserve (34°05′38″ N, 118°39′26″ W) in southern California. The soil is a gravelly sandy loam, covered with 2 cm of leaf litter from a coast live oak tree (*Quercus agrifolia*). The site received 2 mm of precipitation the day before the measurements started. The experimental setup was largely identical to that used at SGP (see Maseyk et al., 2014). Further details on the site and data are provided in Sun et al. (2015).

2.4.2 Site-specific parameters

Site-specific parameters are summarized in Table 2. We used site-specific values for soil porosity that were constant with depth except in the top few centimeters when there is loose topsoil. Soil porosity is estimated as $0.50\,\mathrm{m^3\,m^{-3}}$ at the SGP site from the maximum observed soil moisture (Fischer et al., 2007; Maseyk et al., 2014), but that in the top 2 cm is assumed to be $0.60\,\mathrm{m^3\,m^{-3}}$ as the topsoil is looser due to agricultural activity. At the SR site, soil porosity was measured as $0.35\ \mathrm{m^3\,m^{-3}}$. We assume the field capacity (θ_{FC}) is $0.20\,\mathrm{m^3\,m^{-3}}$ at the SR site based on soil textures (Or and Wraith, 2002). For the parameter b in Eq. (13), we use 4.9 for SR (sandy loam) and 5.3 for SGP (silt loam) based on Clapp and Hornberger (1978).

Soil temperature profiles are modeled with the observations at 5 cm depth. The temperature signals are considered as a superposition of fast varying diurnal signals (T_F) and slowly varying synoptic-scale signals (T_S) (Van Wijk and de Vries, 1963),

$$T(z,t) = T_S + T_F \cdot \exp(-z/z_T)\sin(\omega t + \psi - z/z_T), \quad (26)$$

where z_T is the damping depth for diurnal temperature waves, $\omega = 2\pi\ \mathrm{day^{-1}}$ is the angular frequency, and ψ is the phase constant. z_T is determined from

$$z_T = \sqrt{2\alpha_T/\omega} \quad (27)$$

where α_T ($\mathrm{m^2\,s^{-1}}$) is the soil thermal diffusivity, calculated from soil mineral composition and water content using empirical formulae in Peters-Lidard et al. (1998) and Johansen (1975). Soil thermal diffusivities are $2.5\text{–}5.0 \times 10^{-7}\,\mathrm{m^2\,s^{-1}}$ at the SGP site and $6.8\text{–}8.1 \times 10^{-7}\,\mathrm{m^2\,s^{-1}}$ at the SR site, assuming typical mineral compositions. The thermal diffusivities are translated to average damping depths of 0.11 m (SGP) and 0.14 m (SR), respectively.

For the SR data, we observed that the temperature optimum for COS uptake is $T_{opt} \approx 13\,°\mathrm{C}$ (Sun et al., 2015). This

Table 2. Site-specific parameters (SR: Stunt Ranch, CA; SGP: Southern Great Plains, OK).

Site	θ_{sat} ($m^3\ m^{-3}$)	θ_{FC} ($m^3\ m^{-3}$)	z_T (m) (m)	T_{eq} (°C)	w_{opt} ($m^3\ m^{-3}$)	θ_{lit} ($m^3\ m^{-3}$)	d_{lit} (cm)
SGP	0.50 (0.60 in the top 2 cm)	not used	0.11	10	0.20	not used	not used
SR	0.35	0.20	0.14	15	0.14	0.94	2

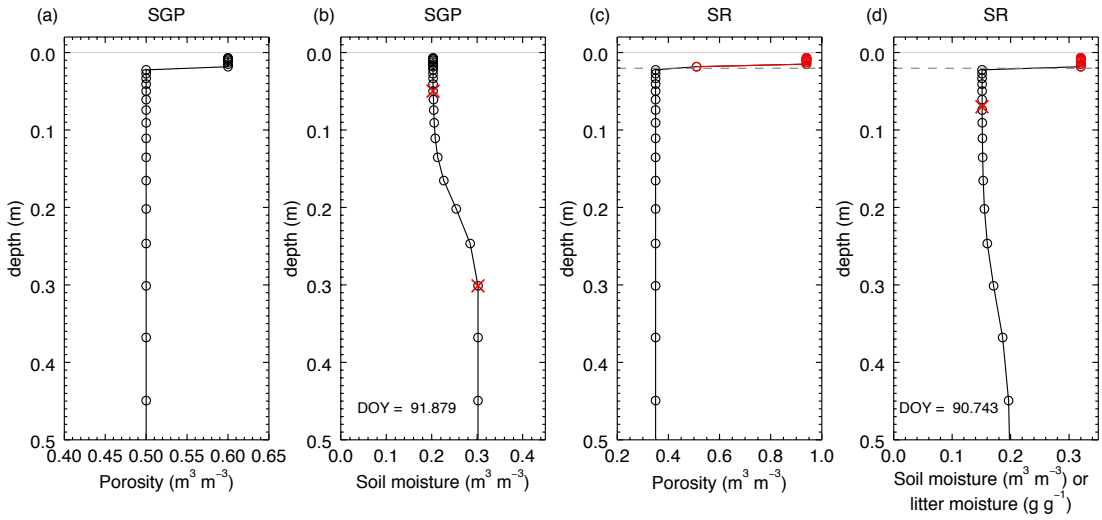

Figure 4. Soil porosity and moisture profiles at the SGP site **(a, c)** and the SR site **(c, d)** in the top 50 cm. Note that in **(c)** and **(d)**, the profiles also show the porosity in the litter layers and litter water content ($g\ g^{-1}$) in red. The dashed lines denote litter–soil interfaces, and the light gray lines represent air–litter interfaces (same for Fig. 7). One computational node near litter–soil interface is interpolated for porosity in order to prevent numerical instability. Measured data of soil moisture at 5 and 30 cm for SGP, and 5 cm for SR, are shown as red crosses.

is reproduced by setting T_{eq} at 15 °C in Eq. (22). For the SGP soil, because COS flux did not show a temperature optimum for uptake during the observed temperature range (7–47 °C) in Maseyk et al. (2014), we set $T_{eq} = 10$ °C (equivalent to $T_{opt} \approx 7$ °C) to get a monotonic relationship with temperature.

Soil moisture was measured at 5 cm depth at both sites, and additionally at 30 cm at SGP. We generate soil moisture profiles for the SGP site by interpolating between the 5 and 30 cm data and assuming constant soil moisture below 30 cm (cf. 1-D simulations with gravity drainage boundary condition in Walker, 1999). For the SR site, we assume soil moisture at 1 m depth is at field capacity ($\theta_{FC}, m^3\ m^{-3}$), and interpolated smoothly between the values at the surface and 1 m depth (Fig. 4). The conditions below 10 cm do not significantly affect surface COS flux according to Fig. 11 (see also Sect. 4.2). The optimum water content for soil COS uptake, w_{opt}, is assumed to be $0.20\ m^3\ m^{-3}$ for SGP soils, corresponding to a threshold for the COS flux-temperature response (Maseyk et al., 2014). For SR soils, we set $w_{opt} = 0.14\ m^3\ m^{-3}$, estimated from lab incubation data of the same soils (Whelan et al., 2015).

Since litter was present at the SR site, litter layers are included in model simulations when validating the model with the SR data set. The 2 cm thick litter layer is represented in the top six grid points. Litter porosity was measured to be $0.94\ m^3\ m^{-3}$. Litter water content (LWC) is an important variable controlling litter COS fluxes. Since LWC was not measured at SR, we test two scenarios: (1) fast decreasing LWC, and (2) slowly decreasing LWC following the precipitation event on the day before the measurements started. We also evaluate the surface COS flux in the absence of litter fluxes.

3 Evaluation results

In the evaluation, soil COS uptake and production capacities ($V_{SU,max}$ and $V_{SP,max}$) are chosen to fit the general trend of observed data. The aim here is to demonstrate that the model can reproduce the data with the proper settings and, thus, has the potential to be applied at large scales. Model performance in the evaluation tests is summarized in Table 3.

Table 3. Summary of model evaluation results.

Site	$V_{SU,max}$ (mol m^{-3} s^{-1})	$V_{SP,max}$ (mol m^{-3} s^{-1})	Mean flux, observed (pmol m^{-2} s^{-1})	Mean flux, modeled (pmol m^{-2} s^{-1})	RMSE	r^2
SGP	1.2×10^{-1}	1×10^{-10}[a], 3.3×10^{-11}[b]	1.0	0.7	2.3	0.688
SR	1×10^{-2}	2×10^{-11}	−1.5	−1.6	0.5	0.869

[a] For the growing season (before DOY 130). [b] For the post-senescence stage (after DOY 134).

3.1 Evaluation against data from the wheat field soil (SGP)

The simulated COS fluxes at the SGP site are generally in good agreement with the observations (Fig. 5), especially the diurnal variations and the transition from uptake to emissions. Model results and the data lie on a 1 : 1 line, albeit with large scatter at high emission fluxes (Fig. 5c). As shown in the distribution of model residuals with respect to surface soil temperature and moisture (Fig. 5d), the model tends to underestimate the high emissions at high temperatures. In the growing season (before DOY 130), the model captures the high uptake instances but tends to underestimate high emission instances at midday. This is mainly because some high emissions are not associated with high soil temperature. During the senescence and post-harvest period (after DOY 134), the model reproduces the strong diurnal variations, except that the midday peak emissions are underestimated. Examples for COS profiles during overall soil COS uptake and emissions show exponential decrease and increase of the COS concentration in soil air with depth, respectively (Fig. 7a).

From the incubation experiments, Maseyk et al. (2014) show that the root-free soil exhibited uptake at −0.21 pmol kgDW^{-1} s^{-1} (−0.4 pgS gDW^{-1} min^{-1}) in the peak growing season but emissions at 0.10 pmol kgDW^{-1} s^{-1} (0.2 pgS gDW^{-1} min^{-1}) in the late growing season and senescence. When translated to the V_{max} parameters as in Eqs. (21) and (24), the incubation data correspond to estimates of $V_{SU,max}$ at 2.6×10^{-2} mol m^{-3} s^{-1} in April and $V_{SP,max}$ at 1.3×10^{-10} mol m^{-3} s^{-1} in May, assuming ambient COS concentration at 2.04×10^{-8} mol m^{-3} (500 pptv, 1 atm, 25 °C), $k_H \sim 1$, and soil dry density of 1.33×10^3 kg m^{-3} estimated from porosity (0.50). These estimates from incubation data are reasonably similar to the model parameters needed to fit the data (Table 3) given that there were only a few incubation experiments.

The observed COS emissions were higher in the senescence and post-harvest stages (after DOY 134) than during the growing season. However, when the temperature dependence is considered, the COS production capacity in the growing season (before DOY 130) must be higher than after harvest to account for the high fluxes under relatively low soil temperatures (< 20 °C) in this period (Fig. 5a, Table 3). We hypothesize that root production of COS may have peaked during the late growing season following increased root sulfate uptake during seed ripening (Zhao et al., 1999), and then decreased during the following senescence stage.

Surprisingly, to simulate the strong diurnal variability of COS emissions in the senescence and post-harvesting stages, the high emissions need to be counteracted by continuing COS uptake, with the same uptake capacity as during the growing season. Without uptake activity, COS would accumulate in the soil column from high production in the daytime and still exhibit high emissions at night. An additional contribution to daytime emissions could have come from photochemical production of COS, as observed for SGP soil in lab incubations (Whelan and Rhew, 2015). However, this would only be a minor component since the maximum photochemical production rate translated to a per area basis was around 2 pmol m^{-2} s^{-1}, less than 10 % of the observed diurnal variability. In addition, photochemical production would not have affected the fluxes measured inside the chamber because it was opaque. However, it may have affected the fluxes measured at the ecosystem scale (Billesbach et al., 2014; Maseyk et al., 2014). Hence, photochemical production will be included in a future model version.

3.2 Evaluation against data from the oak woodland soil (SR)

The observation period at SR started with a rain event and thus at high LWC. We set the starting LWC to 0.32 g g^{-1} to fit the observed high uptake fluxes and simulated a rapid water loss (Fig. 8b) due to strong evaporation at typically warm and sunny conditions. The LWC was assumed to decrease to 0.06 g g^{-1} following an exponential decay function. This assumption fits well with the observed fluxes, both for the diurnal variations and the overall trend (Fig. 6). As an alternative, we used a scenario with slowly decreasing LWC (Fig. 8b), or assuming no litter flux at all. In the first case, the uptake during the dry period was overestimated, whereas the no-litter flux scenario did not reproduce the general trend, even after soil uptake capacity was increased by 10-fold to compensate for the missing litter uptake (Fig. 8a). The soil

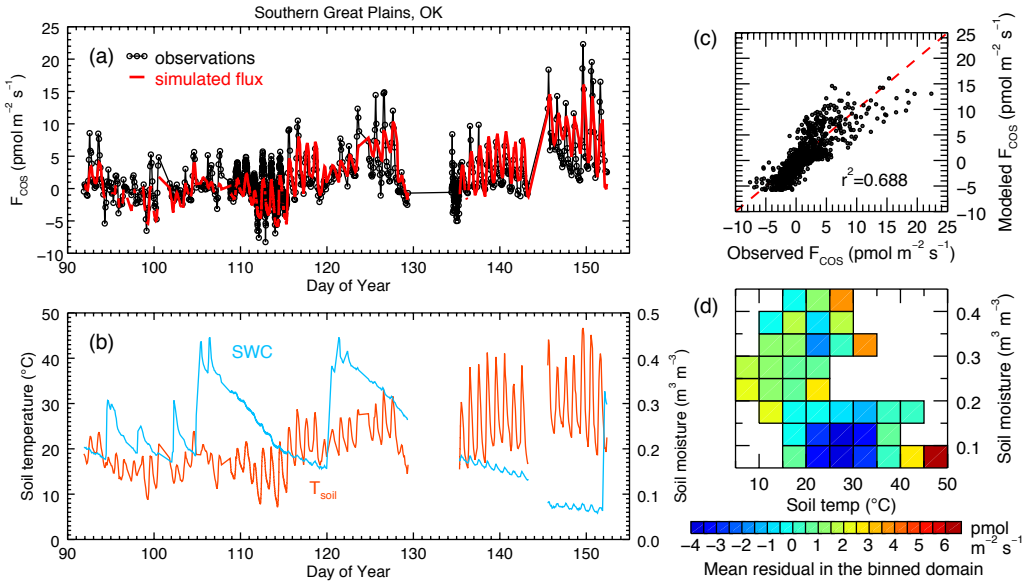

Figure 5. **(a)** Observed COS fluxes (black) and modeled COS fluxes (red) at the Southern Great Plains site. **(b)** Surface soil temperature and moisture at the site during the same period. **(c)** Model vs. data for COS fluxes. **(d)** Mean residuals (observed − modeled) binned by 5 °C soil temperature and 0.05 m^3 m^{-3} soil moisture steps.

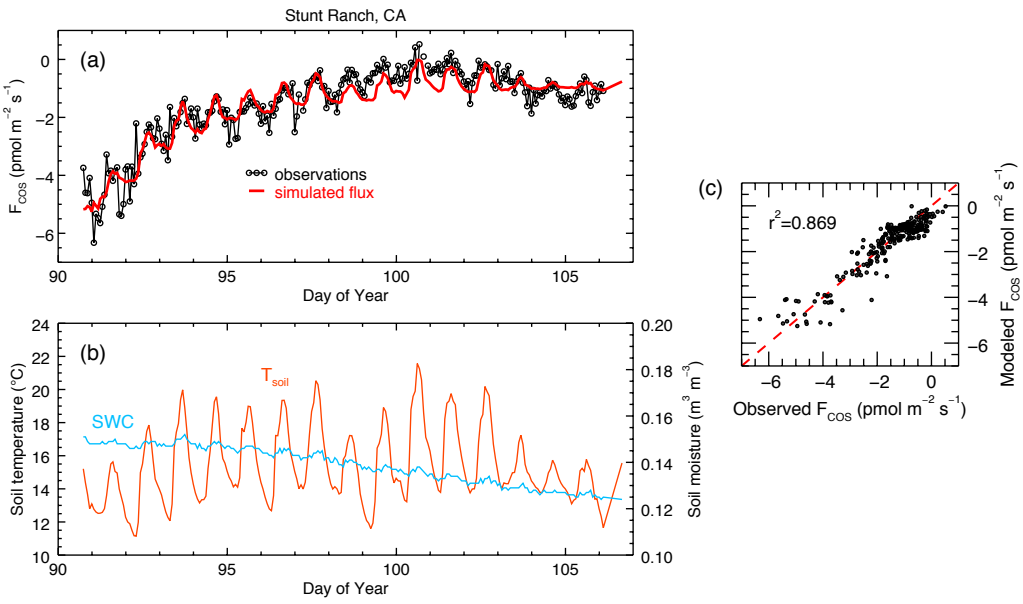

Figure 6. **(a)** Observed COS fluxes (black) and modeled COS fluxes (red) at the Stunt Ranch site. **(b)** Surface soil temperature and moisture at the site during the same period. **(c)** Model vs. data for COS fluxes.

moisture change in this period was not strong enough to drive the overall trend from strong uptake to weak uptake.

The simulated COS profiles show that the presence of litter layers on top of the soil reduces the COS supply available to the soil, especially when there is strong uptake in the litter layers, thus limiting the contribution of soil uptake to the overall surface uptake (Fig. 7b). When LWC is low and litter uptake is weak, this limiting effect is not significant.

4 Discussion

4.1 Sensitivity tests: diffusion-controlled uptake

Laboratory studies have found that soil COS uptake has an optimum at 19–30 % water-filled pore space fraction (WFPS) and approaches zero as WFPS becomes higher (Kesselmeier et al., 1999; Van Diest and Kesselmeier, 2008). We con-

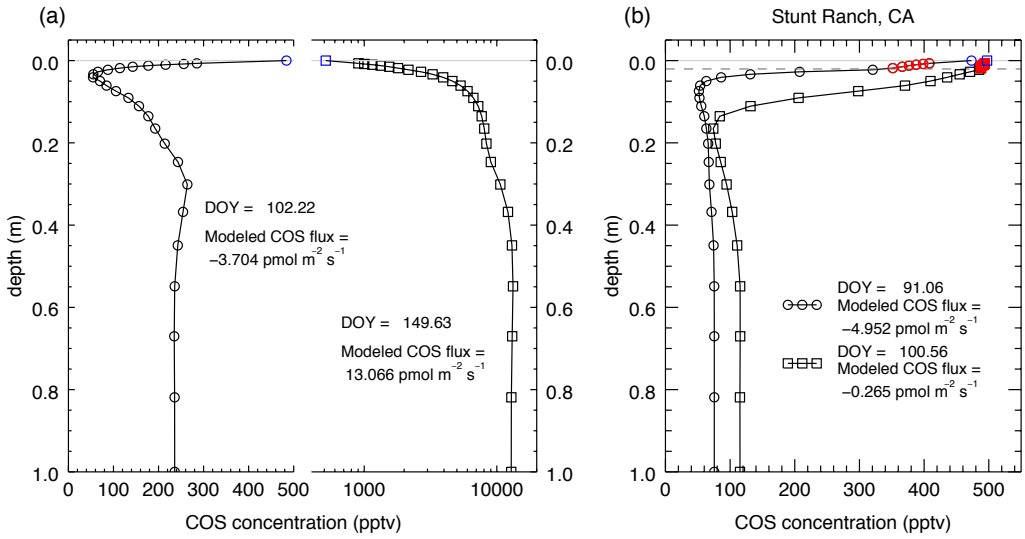

Figure 7. Typical simulated profiles of COS concentration. **(a)** COS profiles of a strong uptake case (circles) and a strong emission case (squares) at SGP. The right side of the x axis is on logarithmic scale. **(b)** COS profiles during the wet period (circles) and the dry period (squares). Blue color is used for the atmospheric concentrations, and red for the concentrations in the litter layers in **(b)**.

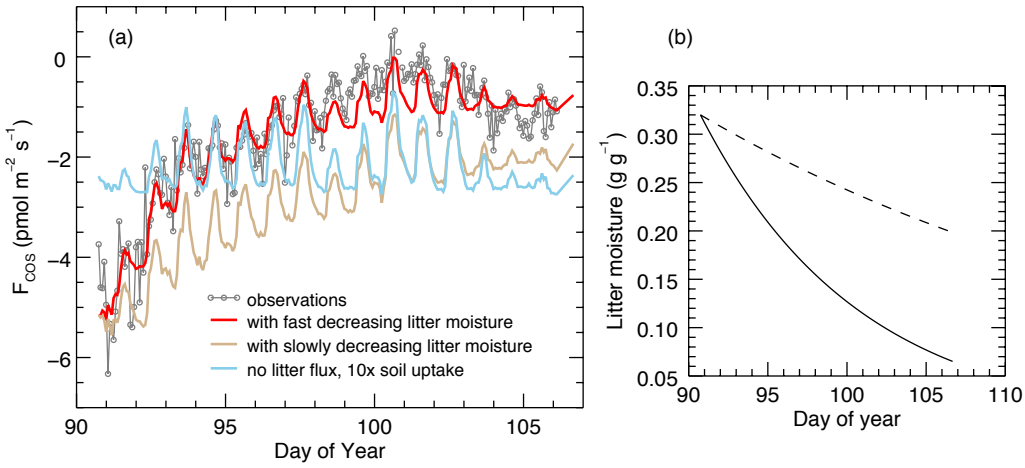

Figure 8. (a) Simulated COS fluxes at the Stunt Ranch site for three scenarios, compared with the observations: fast decreasing litter moisture (red), slowly decreasing litter moisture (light brown), and no litter flux but 10× soil uptake (light blue). **(b)** Changes in litter water content for the fast loss (solid) and slow loss (dashed) scenarios.

ducted a set of idealized simulations to find what factors control such dependence. Based on model results, the shape of the surface flux vs. soil moisture curve is the net result of two competing effects: with increasing soil moisture, the higher microbial activity is counteracted by stronger diffusion limitation. The resultant surface COS uptake has an optimum value of 20 % WFPS, much lower than the optimum value of microbial uptake per se (Fig. 9). The shape of the microbial activity curve is not important at high soil water content where the diffusion limitation is dominant.

We also show that for diffusion-controlled, concentration-dependent uptake, the surface flux does not increase linearly with soil COS uptake capacity ($V_{SU,max}$) but follows a logarithmic relationship (Fig. 10). Hence, if we can constrain the range of soil COS uptake capacity from laboratory experiments, the uncertainty in fluxes arising from this parameter would not be dominant. The non-linear increase also shows that empirical methods that assume a linear response of fluxes to soil COS uptake capacity would not give accurate results.

4.2 Advantages of a depth-resolved model

One of the main advantages of using a depth-resolved model is that it enables the analysis of changes in uptake and production capacities over time, or between sites. For exam-

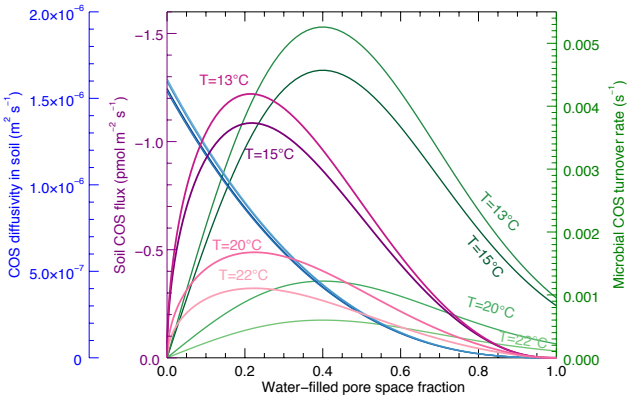

Figure 9. Modeled sensitivity of surface soil COS uptake to water-filled pore space fraction (purple) at soil temperatures of 13, 15, 20 and 22 °C, ambient COS mixing ratio of 500 pmol mol^{-1}, and $V_{SU,max} = 10^{-2}$ mol m^{-3} s^{-1} as in Eq. (21). Soil porosity is set at 0.35 m^3 m^{-3}, and T_{opt} is about 13 °C. Only soil COS uptake activity is included in these simulations. Also shown are the two model variables that dominate the simulated flux response, the effective soil COS diffusivities (blue) and microbial COS uptake turnover rates (green) at the same soil temperatures. Note the y axis of soil COS flux is reversed to show the uptake.

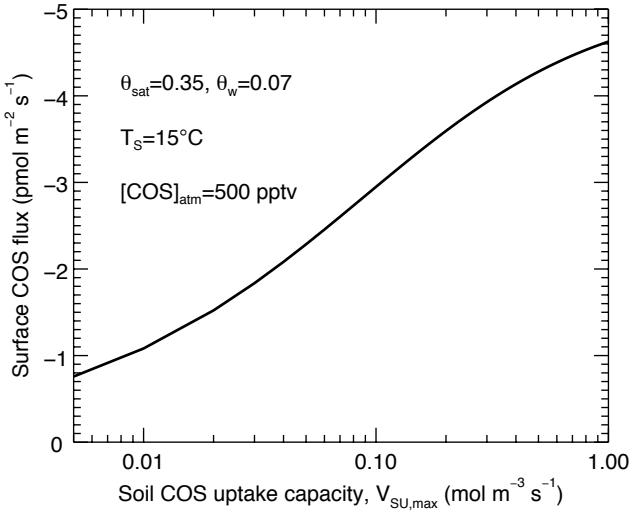

Figure 10. An idealized numerical experiment to test the sensitivity of COS flux to soil COS uptake capacity, with $\theta_{sat} = 0.35$ m^3 m^{-3}, $\theta_w = 0.07$ m^3 m^{-3}, soil temperature at 15 °C, and ambient COS concentration at 500 pmol mol^{-1}. Note that the x axis is in logarithmic scale and the y axis is reversed for showing COS uptake.

ple, an unexpected finding was that the production capacity parameter at SGP needed to be decreased after the senescence stage (from 1×10^{-10} to 3.3×10^{-11} mol m^{-3} s^{-1}; Table 3). Surface COS emissions strongly increased after senescence, but were associated with much higher temperatures. The post-senescence decrease in production capacity indicates that soil COS production may be related to plant activity. We also found that during the period of strong surface COS emissions after the harvest at SGP, the pronounced diurnal variations required the same soil COS uptake capacity as during the growing season, indicating that soil COS uptake does not directly depend on plant activity. Soil COS uptake could be partly abiotic (Liu et al., 2008, 2010b) or largely due to microbial activity (Kesselmeier et al., 1999) but, even in the latter case, may not respond quickly to changes in plant cover.

The uptake and production parameters that best fit at each site and during distinct phenological periods can be obtained by optimization procedures used with a particular soil data set, another significant advantage of a depth-resolved model. Given reasonable initial guesses of the uptake and production parameters, the optimization runs iteratively over the data with the gradient descent or Newton's method until the minimal sum of square errors is attained. An example of data optimization applied to the SR data set is in Sun et al. (2015).

We found that soil COS uptake is largely determined by activity in the top 10 cm of the soil. For each layer, we calculated how much the surface uptake would increase as a result of increasing the COS uptake capacity ($V_{SU,max}$) in that layer by a factor of 10 (Fig. 11). Surface uptake is sensitive to

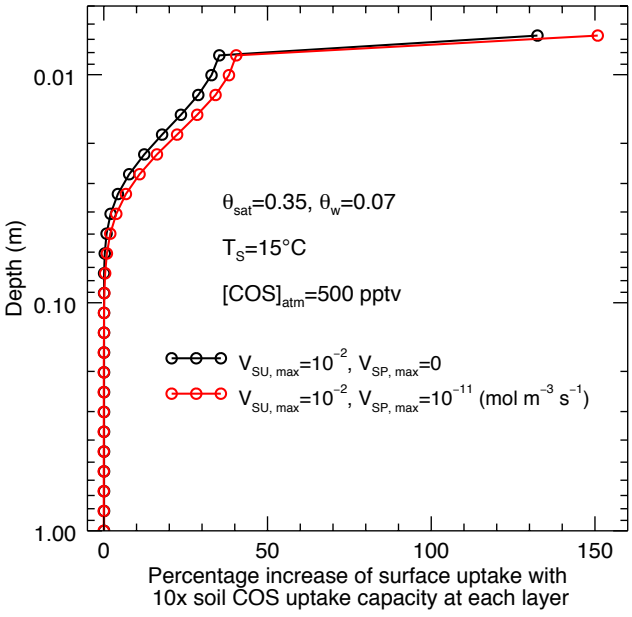

Figure 11. Increase of surface COS uptake (in percentage) from 10-fold changes of $V_{SU,max}$ at each depth. The black line shows the changes for an uptake-only case ($V_{SU,max} = 10^{-2}$ mol m^{-3} s^{-1}), while the red line shows the changes when both uptake and source activities are included ($V_{SU,max} = 10^{-2}$ mol m^{-3} s^{-1}, $V_{SP,max} = 10^{-11}$ mol m^{-3} s^{-1}, but the soil is still a sink). Soil conditions are the same as for Fig. 10.

$V_{SU,max}$ changes in the top 10 cm, even though the layer sizes are the smallest, but not sensitive to changes below 10 cm. Thus, physical parameters in the top layers of the soil are

most important for soil COS fluxes. On the other hand, it also means that information on sources and sinks of COS in the deeper soil cannot be obtained from surface flux measurements.

4.3 Which biome-specific parameters are needed for a global simulation?

The COS flux model can be integrated into more comprehensive land surface models (e.g., CLM4.5 and SiB3) to simulate global fluxes. Soil temperature and moisture are usually generated from prognostic equations in these models. Litter layers would need to be added as they are often not represented separately but embedded in soil layers as soil organic carbon (e.g., in CLM4.5). Several parameters may be biome-specific: (1) the uptake and production capacities of COS ($V_{SU,max}$, $V_{SP,max}$); (2) the optimum temperature and moisture of soil COS uptake (T_{opt}, w_{opt}); (3) the Q_{10} parameter of COS production from microbial, root, or abiotic sources; and (4) the function form of litter COS uptake.

The V_{max} parameters should be controlled by microbial biomass and enzyme content in the soil, which in turn are related to soil physical state and organic carbon content. These parameters can be estimated by optimizing model results against field data. The T_{opt} and w_{opt} parameters can be determined from laboratory experiments, and extended to soils in similar environments, considering that they are likely related to local climate regimes and soil hydrology. Root COS production as a function of temperature needs to be determined from laboratory experiments. More studies are also needed to constrain litter COS fluxes and how they change with litter type, level of litter degradation, and litter moisture content and temperature. With more field observations and lab incubations, we expect that a database of these parameters in different biomes will be constructed for regional and global simulations of soil COS fluxes.

5 Conclusions

This study presents a mechanistic diffusion–reaction model coupling physics and biogeochemistry to simulate soil COS flux, as well as its evaluation with field data. The model explicitly accounts for diffusion in the soil column, COS production, and COS exchange in the litter layer. The model reproduced well-observed fluxes at two sites and has enabled us to gain novel (and unexpected) insights such as the higher COS production capacity at SGP during the growing season despite lower soil COS emissions, and the continuing COS uptake capacity required to partly counteract the large COS emissions at SGP after harvest. We also demonstrate that diffusion must be considered to accurately simulate surface COS fluxes. Diffusion control on surface uptake is evident in its sensitivity to soil water content and the sub-linear response of uptake flux to soil COS uptake capacity. For large-scale simulations of soil COS fluxes, further lab and field studies are needed to establish a database of soil and litter COS uptake and production capacities and parameters for typical soil types across key biomes.

Appendix A: List of variables and parameters

Table A1. List of variables and parameters.

	Value and unit	Description	Reference
Physical and biological constants			
D_m	1.337×10^{-5} m^2 s^{-1}	COS–air mass diffusivity at 25 °C	Massman (1998), Seibt et al. (2010)
T_{ref}	298.15 K	Reference temperature	
R	8.3145 J K^{-1} mol^{-1}	Universal gas constant	
$k_H(T)$	mol mol^{-1}	Henry's law constant of COS	This study, data from Elliott et al. (1989)
K_m	1.9 mol m^{-3}	Michaelis–Menten constant for COS hydrolysis by carbonic anhydrase	Ogawa et al. (2013)
Soil and litter properties			
θ_a	m^3 m^{-3}	Volumetric air content	
θ_w or w	m^3 m^{-3}	Volumetric water content	
θ_{sat}	m^3 m^{-3}	Soil porosity	
θ_{lit}	0.94 m^3 m^{-3}	Litter porosity	
θ_{FC}	m^3 m^{-3}	Field capacity	Or and Wraith (2002)
T	K	Soil or litter temperature	
T_S	K	Slowly varying component of soil temperature	
T_F	K	Fast varying component of soil temperature	
T_L	K	Litter temperature	
w_L	g g^{-1}	Litter water content	
D	m^2 s^{-1}	COS diffusivity in soil	Moldrup et al. (2003)
z_T	m	Damping depth for diurnal temperature waves	
α_T	m^2 s^{-1}	Soil thermal diffusivity	Peters-Lidard et al. (1998), Johansen (1975)
COS solubility model			
μ_g	J mol^{-1}	Chemical potential of COS in gas phase	
μ_{aq}	J mol^{-1}	Chemical potential of COS in aqueous phase	
$\mu_g^{\ominus}$	J mol^{-1}	Chemical potential of COS in gas phase under a chosen standard condition	
μ_{aq}^*	J mol^{-1}	Chemical potential of COS in aqueous phase under a chosen standard condition	
c_g	mol m^{-3}	Gaseous concentration of COS	
c_{aq}	mol m^{-3}	Aqueous concentration of COS	
ϕ	dimensionless	Fugacity coefficient	
γ	dimensionless	Activity coefficient	
p	atm	Partial pressure of COS	
$p^{\ominus}$	1 atm	Standard pressure	
T_0	273.15 K	Standard temperature	
x	dimensionless	Molar fraction of COS in aqueous phase	
ρ_w	1×10^3 kg m^{-3}	Density of water	
M_w	18.016 g mol^{-1}	Molar mass of water	
$k_{H,xp}$	atm^{-1}	Henry's law constant of COS	
$k_{H,cc}$	mol mol^{-1}	Henry's law constant of COS (dimensionless)	
$\Delta_{sol}H_m$	J mol^{-1}	Standard partial molar enthalpy of COS dissolution	
α	dimensionless	Fitting parameter	
β	dimensionless	Fitting parameter	
Fluxes and model parameters			
F_{SL}	pmol s^{-1} kg^{-1} dry weight	COS fluxes from litter incubation	
U	mol m^{-3} s^{-1}	Soil COS uptake term	
P	mol m^{-3} s^{-1}	Soil COS production term	
C	mol m^{-3}	COS gaseous concentration profile	
k_L	11.56	Factor for moisture dependence of litter COS uptake	Sun et al. (2015)
$V_{LU,max}$	1.68×10^{-3} mol m^{-3} s^{-1}	Litter COS uptake capacity	Sun et al. (2015)
$V_{LP,max}$	1.33×10^{-11} mol m^{-3} s^{-1}	Litter COS production capacity	Sun et al. (2015)
$V_{SU,max}$	mol m^{-3} s^{-1}	Soil COS uptake capacity	
$V_{SP,max}$	mol m^{-3} s^{-1}	Soil COS production capacity	

Code availability

The numerical solver described by Eq. (12) and the main program are written in IDL, a proprietary software licensed by Exelis VIS (Boulder, CO, USA). Other statistical analysis and data visualization are performed in the R Language. The code (version 1.0) and the input files are available upon request.

The Supplement related to this article is available online at doi:10.5194/gmd-8-3055-2015-supplement.

Acknowledgements. We thank Mary Whelan, Joe Berry and Ian Baker for valuable discussions. This study was supported by a China Scholarship Council (CSC) fellowship to W. Sun, and the European Research Council (ERC) Starting Grant no. 202835 to U. Seibt.

Edited by: C. Sierra

References

Asaf, D., Rotenberg, E., Tatarinov, F., Dicken, U., Montzka, S. A., and Yakir, D.: Ecosystem photosynthesis inferred from measurements of carbonyl sulphide flux, Nat. Geosci., 6, 186–190, doi:10.1038/ngeo1730, 2013.

Berkelhammer, M., Asaf, D., Still, C., Montzka, S., Noone, D., Gupta, M., Provencal, R., Chen, H., and Yakir, D.: Constraining surface carbon fluxes using in situ measurements of carbonyl sulfide and carbon dioxide, Global Biogeochem. Cy., 28, 161–179, doi:10.1002/2013GB004644, 2014.

Berry, J., Wolf, A., Campbell, J. E., Baker, I., Blake, N., Blake, D., Denning, A. S., Kawa, S. R., Montzka, S. A., Seibt, U., Stimler, K., Yakir, D., and Zhu, Z.-X.: A coupled model of the global cycles of carbonyl sulfide and CO_2: A possible new window on the carbon cycle, J. Geophys. Res.-Biogeo., 118, 842–852, doi:10.1002/jgrg.20068, 2013.

Billesbach, D. P., Berry, J. A., Seibt, U., Maseyk, K., Torn, M. S., Fischer, M. L., Abu-Naser, M., and Campbell, J. E.: Growing season eddy covariance measurements of carbonyl sulfide and CO_2 fluxes: COS and CO_2 relationships in Southern Great Plains winter wheat, Agr. Forest Meteorol., 184, 48–55, doi:10.1016/j.agrformet.2013.06.007, 2014.

Bird, R. B., Stewart, W. E., and Lightfoot, E. N.: Transport phenomena, John Wiley & Sons, Inc., Hoboken, NJ, 2nd Edn., 2002.

Campbell, J. E., Carmichael, G. R., Chai, T., Mena-Carrasco, M., Tang, Y., Blake, D. R., Blake, N. J., Vay, S. A., Collatz, G. J., Baker, I., Berry, J. A., Montzka, S. A., Sweeney, C., Schnoor, J. L., and Stanier, C. O.: Photosynthetic Control of Atmospheric Carbonyl Sulfide During the Growing Season, Science, 322, 1085–1088, doi:10.1126/science.1164015, 2008.

Clapp, R. B. and Hornberger, G. M.: Empirical equations for some soil hydraulic properties, Water Resour. Res., 14, 601–604, doi:10.1029/WR014i004p00601, 1978.

Conrad, R. and Meuser, K.: Soils contain more than one activity consuming carbonyl sulfide, Atmos. Environ., 34, 3635–3639, doi:10.1016/S1352-2310(00)00136-9, 2000.

Crank, J. and Nicolson, P.: A practical method for numerical evaluation of solutions of partial differential equations of the heat-conduction type, Math. Proc. Cambridge Philos. Soc., 43, 50–67, doi:10.1017/S0305004100023197, 1947.

Daniel, R. M., Peterson, M. E., Danson, M. J., Price, N. C., Kelly, S. M., Monk, C. R., Weinberg, C. S., Oudshoorn, M. L., and Lee, C. K.: The molecular basis of the effect of temperature on enzyme activity, Biochem. J., 425, 353–360, doi:10.1042/BJ20091254, 2010.

De Bruyn, W. J., Swartz, E., Hu, J. H., Shorter, J. A., Davidovits, P., Worsnop, D. R., Zahniser, M. S., and Kolb, C. E.: Henry's law solubilities and Śetchenow coefficients for biogenic reduced sulfur species obtained from gas-liquid uptake measurements, J. Geophys. Res., 100, 7245–7251, doi:10.1029/95JD00217, 1995.

Durran, D. R.: Numerical Methods for Fluid Dynamics: With Applications to Geophysics, Springer-Verlag, New York, 2nd Edn., 2010.

Elliott, S., Lu, E., and Rowland, F. S.: Rates and mechanisms for the hydrolysis of carbonyl sulfide in natural waters, Environ. Sci. Technol., 23, 458–461, doi:10.1021/es00181a011, 1989.

Fischer, M. L., Billesbach, D. P., Berry, J. A., Riley, W. J., and Torn, M. S.: Spatiotemporal variations in growing season exchanges of CO_2, H_2O, and sensible heat in agricultural fields of the Southern Great Plains, Earth Interact., 11, 1–21, doi:10.1175/EI231.1, 2007.

Johansen, O.: Thermal conductivity of soils, PhD thesis, Trondheim, Group for Thermal Analysis of Frost in the Ground, Institute for Kjøleteknikk, Norway, translated by: Rosetta Stone, Nashua, N. H. for US Army Cold Regions Research and Engineering Laboratory, 1977, 1975.

Kesselmeier, J. and Hubert, A.: Exchange of reduced volatile sulfur compounds between leaf litter and the atmosphere, Atmos. Environ., 36, 4679–4686, doi:10.1016/S1352-2310(02)00413-2, 2002.

Kesselmeier, J., Teusch, N., and Kuhn, U.: Controlling variables for the uptake of atmospheric carbonyl sulfide by soil, J. Geophys. Res., 104, 11577–11584, doi:10.1029/1999JD900090, 1999.

Kettle, A. J., Kuhn, U., von Hobe, M., Kesselmeier, J., and Andreae, M. O.: Global budget of atmospheric carbonyl sulfide: Temporal and spatial variations of the dominant sources and sinks, J. Geophys. Res., 107, 4658, doi:10.1029/2002JD002187, 2002.

Liu, J., Geng, C., Mu, Y., Zhang, Y., Xu, Z., and Wu, H.: Exchange of carbonyl sulfide (COS) between the atmosphere and various soils in China, Biogeosciences, 7, 753–762, doi:10.5194/bg-7-753-2010, 2010a.

Liu, Y., He, H., and Ma, Q.: Temperature dependence of the heterogeneous reaction of carbonyl sulfide on magnesium oxide, J. Phys. Chem. A, 112, 2820–2826, doi:10.1021/jp711302r, 2008.

Liu, Y., Ma, J., Liu, C., and He, H.: Heterogeneous uptake of carbonyl sulfide onto kaolinite within a temperature range of 220–330 K, J. Geophys. Res., 115, D24311, doi:10.1029/2010JD014778, 2010b.

Maseyk, K., Berry, J. A., Billesbach, D., Campbell, J. E., Torn, M. S., Zahniser, M., and Seibt, U.: Sources and sinks of carbonyl sulfide in an agricultural field in the Southern Great Plains, Proc.

Natl. Aca. Sci., 111, 9064–9069, doi:10.1073/pnas.1319132111, 2014.

Massman, W., Sommerfeld, R., Mosier, A., Zeller, K., Hehn, T., and Rochelle, S.: A model investigation of turbulence-driven pressure-pumping effects on the rate of diffusion of CO_2, N_2O, and CH_4 through layered snowpacks, J. Geophys. Res., 102, 18851–18863, doi:10.1029/97JD00844, 1997.

Massman, W. J.: A review of the molecular diffusivities of H_2O, CO_2, CH_4, CO, O_3, SO_2, NH_3, N_2O, NO, and NO_2 in air, O_2 and N_2 near STP, Atmos. Environ., 32, 1111–1127, doi:10.1016/S1352-2310(97)00391-9, 1998.

Moldrup, P., Olesen, T., Komatsu, T., Yoshikawa, S., Schjønning, P., and Rolston, D.: Modeling diffusion and reaction in soils: X. A unifying model for solute and gas diffusivity in unsaturated soil, Soil Sci., 168, 321–337, 2003.

Montzka, S., Calvert, P., Hall, B., Elkins, J., Conway, T., Tans, P., and Sweeney, C.: On the global distribution, seasonality, and budget of atmospheric carbonyl sulfide (COS) and some similarities to CO_2, J. Geophys. Res., 112, D09302, doi:10.1029/2006JD007665, 2007.

Ogawa, T., Noguchi, K., Saito, M., Nagahata, Y., Kato, H., Ohtaki, A., Nakayama, H., Dohmae, N., Matsushita, Y., Odaka, M., Yohda, M., Nyunoya, H., and Katayama, Y.: Carbonyl sulfide hydrolase from *Thiobacillus thioparus* strain THI115 is one of the β-carbonic anhydrase family enzymes, J. Am. Chem. Soc., 135, 3818–3825, doi:10.1021/ja307735e, 2013.

Oleson, K. W., Lawrence, D. M., Bonan, G. B., Drewniak, B., Huang, M., Koven, C. D., Levis, S., Li, F., Riley, W. J., Subin, Z. M., Swenson, S., Thornton, P. E., Bozbiyik, A., Fisher, R., Heald, C. L., Kluzek, E., Lamarque, J.-F., Lawrence, P. J., Leung, L. R., Lipscomb, W., Muszala, S. P., Ricciuto, D. M., Sacks, W. J., Sun, Y., Tang, J., , and Yang, Z.-L.: Technical description of version 4.5 of the Community Land Model (CLM), NCAR Technical Report NCAR/TN-503+STR, National Center for Atmospheric Research (NCAR), Boulder, CO, USA, doi:10.5065/D6RR1W7M, 2013.

Or, D. and Wraith, J. M.: Soil Water Content and Water Potential Relationships, in: Soil Physics Companion, edited by: Warrick, A. W., CRC Press, 49–84, 2002.

Peters-Lidard, C., Blackburn, E., Liang, X., and Wood, E.: The effect of soil thermal conductivity parameterization on surface energy fluxes and temperatures, J. Atmos. Sci., 55, 1209–1224, 1998.

Peterson, M. E., Eisenthal, R., Danson, M. J., Spence, A., and Daniel, R. M.: A new intrinsic thermal parameter for enzymes reveals true temperature optima, J. Biological Chem., 279, 20717–20722, doi:10.1074/jbc.M309143200, 2004.

Prandtl, L.: Bericht über Untersuchungen zur ausgebildeten Turbulenz, Z. Angew. Math. Mech, 5, 136–139, 1925.

Sandoval-Soto, L., Stanimirov, M., von Hobe, M., Schmitt, V., Valdes, J., Wild, A., and Kesselmeier, J.: Global uptake of carbonyl sulfide (COS) by terrestrial vegetation: Estimates corrected by deposition velocities normalized to the uptake of carbon dioxide (CO_2), Biogeosciences, 2, 125–132, doi:10.5194/bg-2-125-2005, 2005.

Schenk, S., Kesselmeier, J., and Anders, E.: How does the exchange of one oxygen atom with sulfur affect the catalytic cycle of carbonic anhydrase?, Chemistry – A European Journal, 10, 3091–3105, doi:10.1002/chem.200305754, 2004.

Seibt, U., Kesselmeier, J., Sandoval-Soto, L., Kuhn, U., and Berry, J. A.: A kinetic analysis of leaf uptake of COS and its relation to transpiration, photosynthesis and carbon isotope fractionation, Biogeosciences, 7, 333–341, doi:10.5194/bg-7-333-2010, 2010.

Stimler, K., Montzka, S. A., Berry, J. A., Rudich, Y., and Yakir, D.: Relationships between carbonyl sulfide (COS) and CO_2 during leaf gas exchange, New Phytologist, 186, 869–878, doi:10.1111/j.1469-8137.2010.03218.x, 2010.

Stull, R. B.: An Introduction to Boundary Layer Meteorology, Kluwer Academic Publishers, Dordrecht, Netherlands, 1988.

Sun, W., Maseyk, K., Lett, C., and Seibt, U.: Litter dominates surface fluxes of carbonyl sulfide (COS) in a Californian oak woodland, J. Geophys. Res.-Biogeo., submitted, 2015.

Tang, J. Y. and Riley, W. J.: A new top boundary condition for modeling surface diffusive exchange of a generic volatile tracer: theoretical analysis and application to soil evaporation, Hydrol. Earth Syst. Sci., 17, 873–893, doi:10.5194/hess-17-873-2013, 2013.

Tang, J. Y. and Riley, W. J.: Technical Note: Simple formulations and solutions of the dual-phase diffusive transport for biogeochemical modeling, Biogeosciences, 11, 3721–3728, doi:10.5194/bg-11-3721-2014, 2014.

Ulshöfer, V., Flock, O., Uher, G., and Andreae, M.: Photochemical production and air-sea exchange of carbonyl sulfide in the eastern Mediterranean Sea, Marine Chem., 53, 25–39, doi:10.1016/0304-4203(96)00010-2, 1996.

Van Diest, H. and Kesselmeier, J.: Soil atmosphere exchange of carbonyl sulfide (COS) regulated by diffusivity depending on water-filled pore space, Biogeosciences, 5, 475–483, doi:10.5194/bg-5-475-2008, 2008.

Van Wijk, W. R. and de Vries, D. A.: Periodic temperature variations in a homogeneous soil, in: Physics of plant environment, edited by: Van Wijk, W. R., North Holland Publishing Company, Amsterdam, Netherlands, 102–143, 1963.

Von Hobe, M., Kettle, A., and Andreae, M.: Carbonyl sulphide in and over seawater: summer data from the northeast Atlantic Ocean, Atmos. Environ., 33, 3503–3514, doi:10.1016/S1352-2310(98)00236-2, 1999.

Walker, J. P.: Estimating soil moisture profile dynamics from near-surface soil moisture measurements and standard meteorological data, PhD thesis, The University of Newcastle, New South Wales, Australia, 1999.

Whelan, M. E. and Rhew, R. C.: Carbonyl sulfide produced by abiotic thermal and photodegradation of soil organic matter from wheat field substrate, J. Geophys. Res.-Biogeo., 120, 54–62, doi:10.1002/2014JG002661, 2015.

Whelan, M. E., Hilton, T. W., Berry, J. A., Berkelhammer, M., Desai, A. R., and Campbell, J. E.: Carbonyl sulfide exchange in soils for better estimates of ecosystem carbon uptake, Atmos. Chem. Phys. Discuss., 15, 21095–21132, doi:10.5194/acpd-15-21095-2015, 2015.

Wilhelm, E., Battino, R., and Wilcock, R. J.: Low-pressure solubility of gases in liquid water, Chemical Rev., 77, 219–262, doi:10.1021/cr60306a003, 1977.

Wingate, L., Seibt, U., Maseyk, K., Ogée, J., Almeida, P., Yakir, D., Pereira, J. S., and Mencuccini, M.: Evaporation and carbonic anhydrase activity recorded in oxygen isotope signatures of net CO_2 fluxes from a Mediterranean soil, Global Change Biol., 14, 2178–2193, doi:10.1111/j.1365-2486.2008.01635.x, 2008.

Yi, Z., Wang, X., Sheng, G., Zhang, D., Zhou, G., and Fu, J.: Soil uptake of carbonyl sulfide in subtropical forests with different successional stages in south China, J. Geophys. Res., 112, D08302, doi:10.1029/2006JD008048, 2007.

Zhao, F. J., Hawkesford, M. J., and McGrath, S. P.: Sulphur assimilation and effects on yield and quality of wheat, J. Cereal Sci., 30, 1–17, doi:10.1006/jcrs.1998.0241, 1999.